# Tailoring, Structure, and Activity of Carbon-Supported Nanosized Pt−Cr Alloy Electrocatalysts for Oxygen Reduction in Pure and Methanol-Containing Electrolytes

**Hui Yang, Nicolás Alonso-Vante, Jean-Michel Léger, and Claude Lamy***

*Laboratory of Electrocatalysis, UMR CNRS 6503, University of Poitiers, 40 Avenue du Recteur Pineau, F-86022 Poitiers Cedex, France*

*Received: July 31, 2003; In Final Form: November 4, 2003*

The oxygen-reduction kinetics on Vulcan XC-72 carbon-supported nanosized Pt−Cr alloy catalysts were studied using the porous rotating disk electrode technique in pure and methanol-containing electrolytes. The Vulcan XC-72 carbon-supported Pt−Cr alloy catalysts with different Pt/Cr atomic ratios were prepared via a Pt−carbonyl route. X-ray diffraction data showed that the as-prepared nanosized Pt−Cr alloy catalysts mainly have the disordered structures (solid solution) and that the lattice parameter decreases with the increase in Cr content. Energy-dispersive X-ray analysis indicated that the catalyst compositions are nearly the same as the nominal ones. The obtained Pt−Cr alloy nanoparticles are well dispersed on the surface of carbon with a relatively narrow size distribution. For example, the mean particle size of the as-prepared Pt−Cr (1:1)/C catalyst with 20 wt % metal loading is about 3.1 nm in diameter with a standard deviation of 1.3 nm, and the particle size distribution is relatively narrow. As compared to the Pt/C catalyst, the bimetallic alloy catalysts with the different Pt/Cr atomic ratios showed slightly enhanced mass activity (MA) for the oxygen reduction reaction (ORR); however, the significant enhancement in the specific activity (SA) by a factor of about 1.5−3 for the ORR was found on the Pt−Cr alloy catalysts in pure $HClO_4$ solution. This enhancement in SA of the Pt-based catalysts was correlated to the changes in the lattice parameter and Pt/Cr surface composition. Moreover, the bimetallic Pt−Cr alloy catalysts with the different Pt/Cr atomic ratios exhibited much higher methanol tolerance during the ORR than the Pt/C catalyst. Furthermore, the catalytic activity for methanol oxidation on the Pt−Cr alloy catalysts was much lower than that on the Pt/C catalyst. Thus, the high methanol tolerance of the carbon-supported Pt−Cr alloy catalysts for the ORR can be ascribed to the weak adsorption of methanol induced by the presence of Cr atoms in the alloys.

## 1. Introduction

Proton-exchange membrane fuel cells (PEMFCs) have received considerable attention for transportation applications due to the high energy density, relatively low operating temperatures, zero or low emission of pollutants, and minimal corrosion problems. However, the commercial viability of PEMFCs is still hindered by several problems, including the poor kinetics of cathodic reactions and the high costs of both polymeric electrolyte membrane materials and Pt-based electrocatalysts. It is well known that most of the performance losses due to deviation from the thermodynamic potential of the PEMFC come from the cathode reaction. Thus, there is great room for improvement in oxygen-reduction kinetics.

During the past decade, there has been an increasing interest in the development of direct methanol fuel cells (DMFC) for the applications in transportation and in portable electronic devices[1−4] because the use of methanol as fuel has several advantages in comparison to hydrogen; it is cheap liquid fuel, easily handled, transported, and stored, with a high theoretical energy density.[5,6] Although a lot of progress has been made in the development of DMFC, its performance is still limited by several problems, including the poor kinetics of both anode[7−9] and cathode reactions[10−12] and the crossover of methanol from the anode to the cathode side through the proton-exchange membranes.[13−15] These phenomena lead to high overpotentials on both the anode and cathode sides and, hence, reduction of the cell voltage. Moreover, the crossover effect in the DMFC membrane causes a further decrease in the cathode efficiency due to the occurrence of a mixed potential, which results from the competitive reaction between oxygen reduction and methanol oxidation on the state-of-the-art Pt cathode.[15−19] To avoid this problem, one strategy is the development of novel less-methanol-permeable membranes or modification of the existing membranes, whereas another route is the use of oxygen-reduction catalysts, which are inactive toward methanol oxidation or have a high methanol tolerance.

Various transition-metal macrocycles[17,19−22] and ruthenium-based chalcogenides[23−27] have been tested as methanol-tolerant oxygen cathodes because these compounds are inactive toward the oxidation of methanol. However, the intrinsic catalytic activities of these catalysts for the oxygen-reduction reaction (ORR) are still lower than those of Pt-based catalysts, and the long-term stability under fuel cell operation at high potentials has not been well tested as compared to Pt-based catalysts. Thus, it is necessary to develop novel Pt-based electrocatalysts, which can catalyze the oxygen reduction with limited oxidation of methanol. Previous studies have shown that the use of Pt alloy catalysts could be an efficient route to meet this requirement since the carbon-supported Pt−Cr alloy catalyst (from E-Tek)[28] and bulk Pt−Ni[29] alloy catalyst have been found to exhibit high methanol tolerance during ORR in comparison to pure Pt.

* Corresponding author. Tel: +33-5-49-45-36-28. Fax: +33-5-49-45-35-80. E-mail: claude.lamy@univ-poitiers.fr.

10.1021/jp030948q CCC: $27.50 
Published on Web 01/16/2004

Because of the high overpotential for the ORR under typical fuel cell operating conditions (at least 0.3−0.4 V), Pt alloy catalysts with various transition metals were employed to increase the catalytic activity and to decrease the cost. Many investigations have shown that some Pt-based alloy catalysts,[29−40] such as Pt−M, (where M = Co, Ni, Fe, V, Mn, and Cr), exhibited an enhanced electrocatalytic activity for the ORR compared to Pt alone. The improvement in the ORR electrocatalysis on Pt alloy catalysts has been explained by several factors such as electronic and structural effects.[34,36] Usually, such carbon-supported Pt alloy catalysts were prepared by the impregnation of the second metal on Pt/C and then by alloying at temperatures above 700 °C under inert gas or hydrogen. This heat treatment at high temperatures gives rise to an undesired alloy particle growth, which may result in the decrease in Pt mass activity (MA) for the ORR. Also, the control of the particle size distribution with this preparation method is quite limited. Recently, some groups have reported that such Pt alloy catalysts could be prepared by the coreduction of the metallic salt precursors at low temperatures and that the obtained Pt alloy particle sizes are relatively small.[41,42]

Another alternative way to tailor the nanosized Pt-based alloys for the different purposes is the use of organometallic compounds as precursors.[43−46] By the thermal decomposition or reducing treatment of organometallic precursors, small nanoparticles of metal or alloy with narrow size distribution could be obtained. For example, Sun et al.[43] obtained Pt−Co nanoparticles of about 2 nm with very narrow size distribution from the organometallic precursors. Similarly, nearly monodisperse Pt−Co,[44] Pt−Fe,[45] and Pt−Mn[46] nanoparticles were prepared by the decomposition of organic precursors. Among the various organometallic precursors used, metal−carbonyl complexes are often employed for preparing carbon-supported metal or alloy catalysts. By the thermal decomposition of the Ru−carbonyl precursor in different organic solvents, Alonso-Vante,[24] Schmidt et al.,[25] Dassenoy et al.,[47] and Bron et al.[26] synthesized Ru-based transition-metal chalcogenide clusterlike nanomaterials for the ORR in pure and methanol-containing electrolytes. By the reduction of Pt−Ru−carbonyl molecular precursors, Nasher et al.[48] and Hills et al.[49] prepared carbon-supported bimetallic Pt−Ru alloys with very small particle size and narrow size distribution. More recently, Dickinson et al.[50] developed carbon-supported Pt−Ru alloy catalysts by decomposing the Pt carbonyl and Ru carbonyl in organic solvents. The obtained Pt−Ru catalysts with small particle size and narrow size distribution exhibited good performance for methanol oxidation in comparison to the commercial Pt−Ru/C catalyst. Recently, our group successfully synthesized carbon-supported Pt−Sn alloy catalysts through the carbonyl chemical route.[51] The obtained Pt−Sn alloy catalysts with very small particle size, narrow size distribution, and disordered structure exhibited good performances for electrocatalytic reactions.

It is known that, among the various Pt-based alloy catalysts used for the ORR, the Pt−Cr alloy is stable in acidic and oxidizing media at high temperature,[10,32] whereas the Pt−Cu and Pt−Fe alloys are unstable under fuel cell operating conditions.[52] The main purposes of the present work are to prepare carbon-supported nanosized Pt−Cr alloy catalysts with different Pt/Cr atomic ratios via a Pt−carbonyl route and to study the influences of the composition and structure of the catalyst on its electrocatalytic activity for the ORR in pure and methanol-containing electrolytes.

## 2. Experimental Section

**2.1. Preparation of Vulcan XC-72 Carbon-Supported Nanosized Pt−Cr Alloy Catalysts.** The nanosized Pt−Cr alloy catalysts were prepared via a Pt−carbonyl route, followed by heat treatment in the temperature range of 400−550 °C. Briefly, Pt−carbonyl complexes $[Pt_3(CO)_6]_{\sim 10}^{2-}$ were synthesized using methanol as a solvent through the reaction of $Na_2PtCl_6$ with CO at about 50 °C for 24 h with constant mechanical stirring,[53] but the stoichiometric amount of $CrCl_3$ was simultaneously added before the reaction. For example, for the preparation of the Pt−Cr(2:1)/C catalyst with 20 wt % metal loading, 239.6 mg of $Na_2PtCl_6 \cdot 6H_2O$ (ca. 31.3 wt % of Pt), 30.46 mg of $CrCl_3$, 127.36 mg of $CH_3COONa$, and ca. 25 mL of methanol were added to a 50-mL three-neck flask. The air in the flask was purged by highly pure nitrogen for more than 30 min, followed by CO flushing for 10 min. Thereafter, the system was sealed and filled with CO, and the temperature was raised to 50 °C for 24 h. Experimental results by infrared spectroscopy showed that the resulting solution is a mixture of Pt−carbonyl and Cr salt. After the synthesis of Pt−carbonyl complexes, 339.9 mg of Vulcan XC-72 carbon was added to the mixture and stirred at about 55 °C for more than 6 h. Subsequently, the solvent was removed and the powder was transferred into a glovebox and then subjected to heat treatment at 500 °C under nitrogen for 1 h and under hydrogen for 3 h, respectively. Therefore, we got the Pt−Cr/C alloy catalyst with the Pt/Cr atomic composition of 2:1 and a total metal loading of 20 wt %. We mentioned here that the alloying temperature under hydrogen is about 400−550 °C, which depends on the catalyst composition. After the heat treatment, the sample was washed with water until no chlorine ions were detected and then dried under nitrogen at about 130 °C for 2 h.

**2.2. Physical Characterization of the Nanosized Pt-Based Catalysts.** X-ray diffraction (XRD) measurements of Pt-based carbon-supported catalysts were carried out on a Siemens D5005 X-ray diffractometer ($\theta-\theta$) using Cu K$\alpha$ radiation ($\lambda = 0.15406$ nm). The sample containing ca. 20 mg of catalysts was deposited on a Si wafer cut along the (511) plane. The XRD spectra were obtained using high resolution in the step-scanning mode with a narrow receiving slit (0.5°) with a counting time of 15 s per 0.1°. Scans were recorded in the $2\theta$ range of 30−90°. The identification of the phases was made by referring to the Joint Committee on Powder Diffraction Standards International Center for Diffraction Data (JCPDS-ICDD) database. The lattice parameters were simulated and refined by using the FullProf 98 software. The particle size of the as-prepared catalysts was evaluated by transmission electron microscopy (TEM) using a Philips CM120 microscope equipped with a $LaB_6$ filament. The samples were prepared by placing one drop of the carbon-supported catalysts, which were dispersed in ethanol, on a copper grid covered by carbon film and by evaporating the solvent. The composition of the as-prepared alloy catalysts was determined by energy-dispersive X-ray (EDX) analysis with the TEM microscope using the E-Tek Pt−Cr (1:1, 10 wt %)/C catalyst as a reference on various spots in order to estimate an average composition of the material.

**2.3. Electrode Preparation and Electrochemical Measurements.** Porous electrodes were prepared as described previously.[28] Twenty milligrams of catalysts, 0.5 mL of Nafion solution (5 wt %, Aldrich), and 2.5 mL of ultrapure water were mixed ultrasonically. A measured volume (3 $\mu$L) of this ink was transferred via a syringe onto a freshly polished glassy carbon disk (3 mm in diameter). After the solvents were evaporated overnight at room temperature, the electrode was

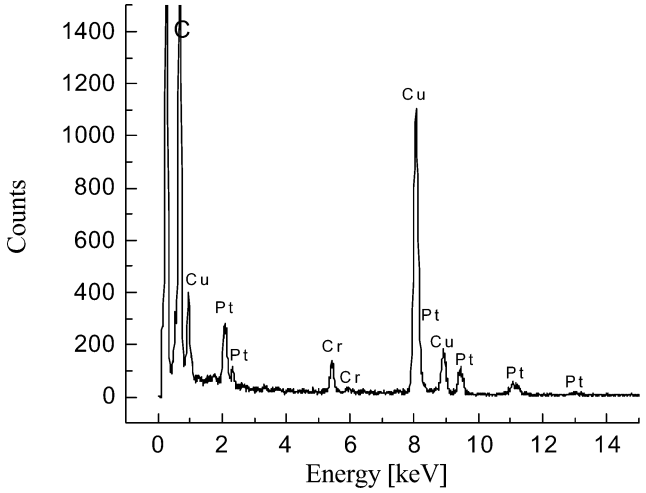


**Figure 1.** Typical EDX spectrum of nanosized Pt−Cr(1:1)/C alloy catalyst with 20 wt % metal loading.

used as the working electrode. Previous study has proved that this method is reproducible and that the utilization of the Pt surface area is close to 100%.[28] Each electrode contained about 56 $\mu$g cm$^{-2}$ of the metal.

All chemicals used were of analytical grade (Alfa Aesar). All the solutions were prepared with ultrapure water (MilliQ, Millipore). Electrochemical measurements were performed using an Autoalab Potentiostat/Galvanostat and a conventional three-electrode electrochemical cell. The counterelectrode was a glassy carbon plate, and a mercury/mercurous sulfate electrode (MSE) was used as the reference electrode, which was connected to the working electrode compartment by a Luggin capillary, but all the potentials are quoted with respect to the reversible hydrogen electrode (RHE). The base electrolyte used was 0.5 M $HClO_4$ or 0.5 M $HClO_4$ + 0.5 M $CH_3OH$. Because of slight contamination from the Nafion solution, the porous electrodes were cycled in 0.5 M $HClO_4$ solution at 50 mV s$^{-1}$ between 0.05 and 1.02 V until reproducible cyclic voltammograms (CVs) were obtained prior to any electrochemical measurements. The upper potential was set to ca. 1.0 V/RHE so that the particle surface change could be avoided. The real surface area of the nanodivided Pt was determined by CO-stripping voltammetry at the scan rate of 20 mV s$^{-1}$.[54] The commonly accepted value is 484 mC cm$^{-2}$ for platinum.[54] The electrochemical activity for the ORR was measured with the rotating disk electrode (RDE) technique (Autolab speed control). High-purity nitrogen or oxygen was used for deaeration of the solutions. During the measurements, a gentle nitrogen or oxygen flow was kept above the electrolyte surface.

All electrochemical experiments were performed in a thermostated cell at a temperature of 20 ± 1 °C.

## 3. Results and Discussion

**3.1. Catalyst Characterization.** The practical composition of the Pt−Cr alloy catalysts was evaluated by EDX analysis (not single-nanoparticle spot-resolved EDX analysis). Figure 1 shows the typical EDX spectrum of the as-prepared Pt−Cr alloy catalyst with the nominal atomic composition of 1:1. It was found that the EDX composition for such a sample in various parts of the nanoparticle powders is about 49.0:51.0, which is very close to the nominal value. The obtained EDX compositions for all the alloy catalysts investigated in this work are shown in Table 1. It can be seen that all the EDX compositions of the as-prepared Pt−Cr alloy catalysts are nearly the same as

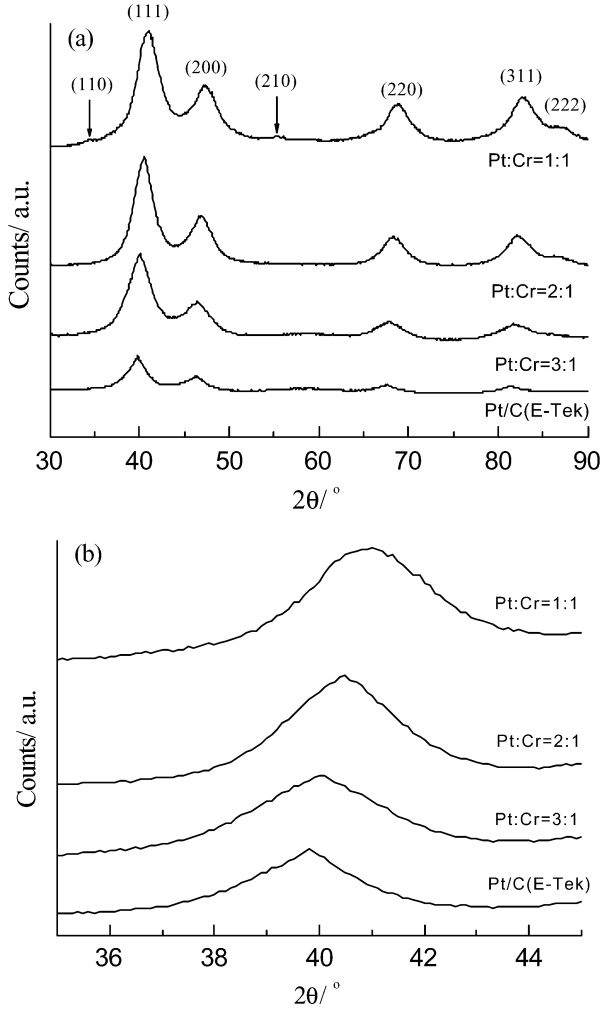


**Figure 2.** X-ray diffraction patterns of the carbon-supported Pt and Pt−Cr alloy catalysts with 20 wt % metal loading with (a) wide scanning and (b) fine scanning of the (111) peak.

**TABLE 1: Composition and Structural Parameters of the Pt/C (E-Tek) and As-Prepared Pt−Cr/C Alloy Catalysts with 20 wt % Metal Loading**

| catalyst | EDX Pt/Cr composition (%) | lattice parameters $a_{fcc}$ (nm) | particle size (nm) from XRD |
|---|---|---|---|
| Pt/C | (100) | 0.3923 | 3.1 |
| Pt:Cr(3:1) | 77.3:22.7 | 0.3895 | 3.5 |
| Pt:Cr(2:1) | 62.7:37.3 | 0.3863 | 3.4 |
| Pt:Cr(1:1) | 49.0:51.0 | 0.3817 | 3.2 |

the nominal values, indicating that Cr can be alloyed with Pt issued from the carbonyl route of synthesis.

Figure 2 shows the XRD patterns of the carbon-supported Pt−Cr alloy catalysts with a metal loading of 20 wt % and the different Pt/Cr atomic ratio, heat treated at 500 °C. For the sake of comparison, the commercial Pt/C catalyst with 20 wt % metal loading (from E-Tek) is also shown in this figure. As indicated in Figure 2a, all the XRD patterns clearly show the five main characteristic peaks of the face-centered cubic (fcc) crystalline Pt (JCPDS card 04-0802), namely, the planes (111), (200), (220), (311), and (222), demonstrating that all the alloy catalysts mainly resemble the single-phase disordered structure (solid solution), which is different from the Pt−Cr(1:1)/C catalyst (10 wt %, from E-Tek) with the ordered Pt−Cr phase structure (data not shown). This difference could be due to the different alloying conditions. These five diffraction peaks in the Pt−Cr alloy catalysts are slightly shifted to higher $2\theta$ values with respect to the corresponding peaks in the Pt/C catalyst and show the effect

of increasing amounts of Cr in the Pt−Cr alloy catalysts. The higher angle shifts of the Pt peaks, which can be clearly seen in Figure 2b, reveal the alloy formation between Pt and Cr, which was caused by the incorporation of Cr in the fcc structure of Pt. No peak for pure Cr and its oxides was found. In addition to the five main characteristic peaks of the Pt fcc structure, two weak peaks located at the $2\theta$ values of approximately 32.8 and 53.2° were found for the Pt−Cr(1:1)/C catalyst, which are assigned to the superlattice planes of the (110) and (210) crystal faces, as indicated in the figure,[55] showing the formation of an ordered Pt−Cr alloy phase with this catalyst. For the Pt−Cr-(3:1)/C and Pt−Cr(2:1)/C samples, however, no superlattice reflections were detected, which may be related to the difference in the Cr amount with these samples. Although the superlattice lines were observed for the as-prepared Pt−Cr (1:1)/C catalyst, the ratio of the ordered phase to disordered phases is very small, indicating that the main phase with this sample is still the solid solution with Pt fcc structure. The presence of the ordered phase leads to the evidence that Cr is completely alloyed with Pt, assessing that the synthesis procedure via the carbonyl route is a good method for preparing the carbon-supported Pt−Cr alloy catalysts. As reported in the literature,[32,33,56] the superlattice phases are generally formed at temperatures above 900 °C for supported Pt−Cr catalysts. However, the superlattice lines are found for the as-prepared Pt−Cr (1:1)/C, via a carbonyl route, thermally treated at about 500 °C. This may be due to the differences in the metallic precursors.

The lattice parameters ($a_{fcc}$) of Pt−Cr alloy catalysts, which reflect the formation of the solid solution, are calculated using the (111) crystal face and given in Table 1. The obtained lattice parameters for all the Pt−Cr alloy catalysts are smaller than those for the Pt/C and decrease with the increase of Cr content, indicating the lattice contraction after alloying. In fact, the decrease in the lattice parameters within the alloy catalysts reflects the progressive increase in the conversion of Cr into the alloyed state. The nearly linear relationship between the lattice parameter and EDX composition (plot not shown) again confirmed that Cr is alloyed with Pt within all the as-prepared Pt−Cr catalysts. In fact, such a linear dependence also reflects the Vegard's law validity for solid solution.

The average size of the Pt−Cr alloy nanoparticles was estimated by using the Scherrer's equation[57] $d = 0.94\lambda_{k\alpha1}/B_{(2\theta)} \cos\theta_B$, where $d$ is the average particle diameter, $\lambda_{k\alpha1}$ is the wavelength of X-ray radiation (0.154056 nm), $\theta_B$ is the angle of the (220) peak, and $B_{(2\theta)}$ is the width in radians of the diffraction peak at half height. The obtained average particle sizes of all the catalysts are given in Table 1. From the table, it can be found that the mean particle size for all Pt−Cr alloy catalysts prepared through the carbonyl route is smaller than that of the Pt−Cr(1:1)/C catalyst (10 wt %, from E-Tek), which has a mean particle size of about 4.2 nm.[28] The mean particle size slightly decreases with the increase of Cr content. In addition, it is very interesting that all the catalysts have nearly the same structure and similar particle size (also see TEM result in Table 2); thus, under these conditions, it is suitable to compare their electrocatalytic activity for the ORR.

Figure 3 shows the TEM images of the carbon-supported Pt−Cr alloy catalysts with the different Pt/Cr atomic ratio and the corresponding particle size distribution histograms based on the observation of more than 1000 nanoparticles. As can be seen, the Pt−Cr alloy nanoparticles are well dispersed on the surface of the support with a narrow particle size distribution. For the Pt−Cr (1:1) alloy catalyst, the obtained mean particle size is about 3.1 ± 1.3 nm in diameter with a relatively narrow size distribution. As the Cr content decreases within the catalyst, the mean particle size for the Pt−Cr (2:1) and Pt−Cr (3:1) alloy catalysts increases to about 3.3 ± 1.2 and 3.4 ± 1.0 nm, respectively. These values are in good agreement with the XRD data. The obtained average particle size in diameter and the standard deviation for all the catalysts are given in Table 2. Assuming that all particles are spherical, the volume surface mean diameter ($d_{vs}$) of each catalyst sample could be obtained from the particle size distribution. Then, the surface average dispersion ($D$), which is defined as the ratio of the surface atoms to the total atoms within the nanoparticles, was also calculated using the relationship between relative particle size ($d_{rel} = d_{vs}/d_{at}$, where $d_{at}$ is the atomic diameter) and $D$ ($D = 2.64/(d_{vs})^{0.81}$) is based on the Borodzinski et al. model.[58] In fact, this model considers the particle size effects and is thus more accurate than other commonly used methods. The resulting $D$ values for all catalysts are given in Table 2. As described above, the alloying temperature for Pt−Cr alloys via the carbonyl pathway is much lower than that of previously reported results,[56] which may be favorable for the formation of the small alloy nanoparticles together with a narrow size distribution. Therefore, the catalyst preparation procedure via a carbonyl route seems to be a good method to obtain nanosized alloy catalysts with a narrow particle size distribution and thus a good dispersion.

**TABLE 2: Particle Size, Dispersion, and Surface Composition of the Pt−Cr Alloy Catalysts**

| catalyst | particle size (nm) from TEM | dispersion $D$ (%) | Pt real surface area ($m^2\ g^{-1}$) | Pt/Cr surface composition (%) |
|---|---|---|---|---|
| Pt/C | 2.8 ± 2.0[a] | 28.0 | 59.3 | (100) |
| Pt:Cr(3:1) | 3.4 ± 1.0 | 29.9 | 53.5 | 74:26 |
| Pt:Cr(2:1) | 3.3 ± 1.2 | 30.6 | 45.8 | 54:46 |
| Pt:Cr(1:1) | 3.1 ± 1.3 | 31.7 | 30.8 | 30:70 |

[a] From ref 28.

It is well known that the real surface area of Pt within the catalysts is an important parameter to determine the electrocatalytic properties for the ORR and methanol oxidation since these two reactions are surface-sensitive. To determine the real surface area of the platinum within the catalysts, the CO-stripping voltammetry was employed according to the procedure described in ref 54. Figure 4 presents a typical CO-stripping voltammogram of our nanodivided alloy catalysts, e.g., Pt−Cr-(2:1)/C in 0.5 M $HClO_4$ at the scan rate of 20 mV $s^{-1}$. From the figure, one well-defined single CO oxidation peak was found, which was present for the other Pt/Cr compositions. From the CO oxidation charge, the real surface area of the Pt/C catalyst and the Pt−Cr alloy catalysts are also listed in Table 2. It can be seen that the real surface area of Pt within the catalysts decreases with the increase in Cr content. From the catalyst loading per geometric electrode area and the dispersion of the catalysts (in Table 2), the surface atomic density can be easily obtained. From the electrochemically active surface area of Pt within the catalysts, the surface Pt atomic density can be calculated. Thus, the Pt/Cr surface composition of the alloy catalysts can be estimated and is also given in Table 2. Assuming that alloying with Cr does not affect the adsorption of CO on platinum surface atoms present on the nanoparticles, the CO-stripping electrochemical analysis reveals that Pt/Cr surface composition is lower than the bulk composition leading to a Cr surface enrichment with the increase of Cr content. Although $H_{upd}$ analysis performed on Pt−Ni(Co) alloy catalysts from E-Tek [38] revealed a similar trend, it is difficult to assess, within our experimental conditions, whether such a phenomenon is due to a segregation effect or not. This latter cannot be,

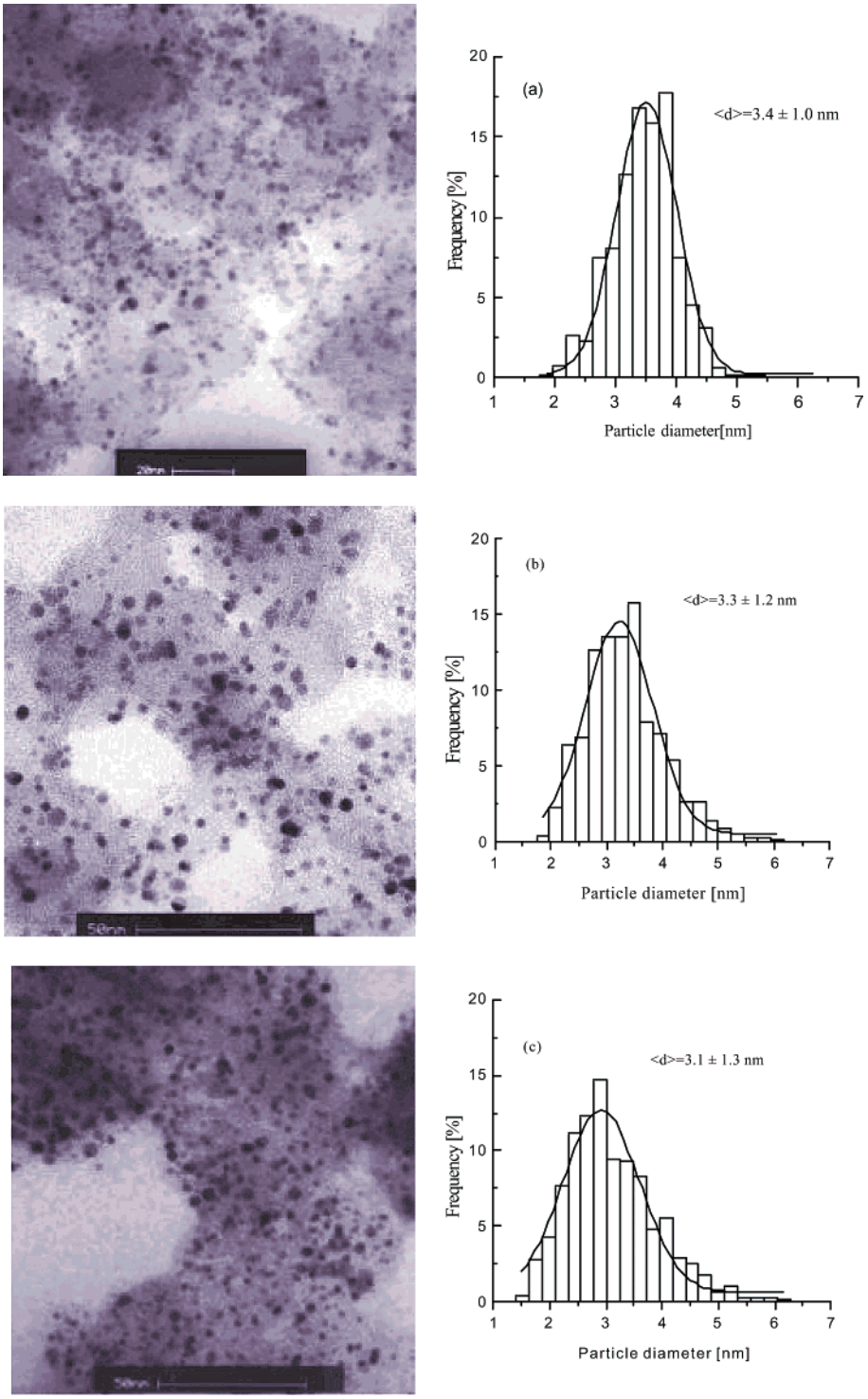


**Figure 3.** TEM images of the (a) Pt−Cr(3:1)/C, (b) Pt−Cr(2:1)/C, and (c) Pt−Cr(1:1)/C catalysts with 20 wt % metal loading and their corresponding particle size-distribution histograms.

however, easily excluded from the nanodivided scale of our supported catalyst.

**3.2. Electrochemical Behavior of the Catalysts for the ORR in Perchloric Acid Electrolyte.** Figure 5 shows the cyclic voltammograms of the Pt/C catalyst and the carbon-supported nanosized Pt−Cr/C alloy catalysts in 0.5 M $HClO_4$ at the scan rate of 50 mV $s^{-1}$ between 0.05 and 1.02 V. From the CV of the Pt/C catalyst, in Figure 5, the hydrogen adsorption/desorption peaks and preoxidation/reduction peaks of the Pt surface on Pt are clearly seen, indicating the presence of polycrystalline Pt. But on the Pt−Cr alloy catalysts, no well-defined hydrogen adsorption/desorption peaks were found, suggesting that the high dispersion of the catalysts with the disordered surface structure was obtained[36] and that their surfaces remain stable in the explored potential interval. In addition, all the Pt/C and Pt−Cr catalysts have a similar double-layer behavior, which is different from the carbon-supported Pt−Co and Pt−Ni samples from E-Tek,[38,39] indicating that all the catalysts have a similar double-layer capacitance. Furthermore, it can be found that the onset of the oxide formation and the peak potential of the oxide reduction (indicated with an arrow in the figure) are also shifted to more positive potentials with the increase of Cr content, indicating that the alloying of Pt with Cr inhibits the chemisorption of OH on the Pt sites at high potentials (above 0.8 V).

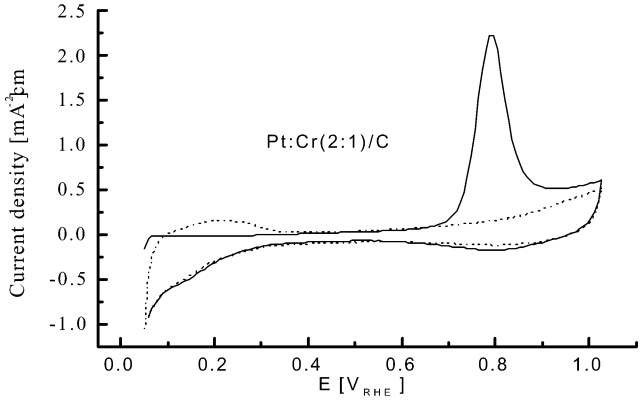


**Figure 4.** CO-stripping voltammograms of the Pt−Cr(2:1)/C catalyst 0.5 M $HClO_4$ at the scan rate of 20 mV/s. Current densities are normalized to the geometric surface area.

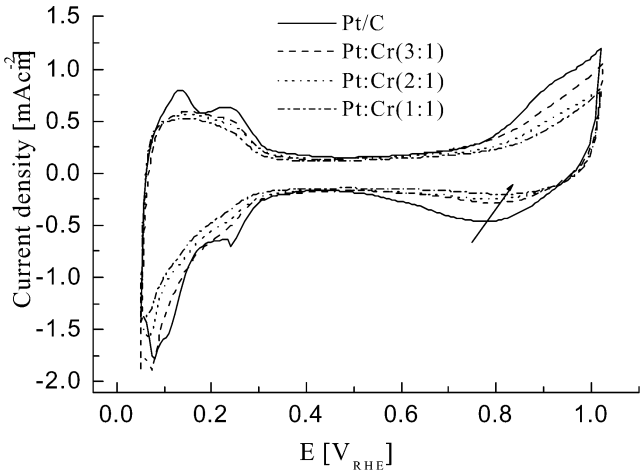


**Figure 5.** Cyclic voltammograms of the Pt/C catalyst and the carbon-supported nanosized Pt−Cr alloy catalysts in 0.5 M $HClO_4$ at the scan rate of 50 mV/s. Current densities are normalized to the geometric surface area.

This may have a beneficial effect on the oxygen adsorption at low overpotential and thus may lead to an enhancement of the ORR kinetics.[35,59] It should be mentioned here that no marked changes in the shape or size of the CVs are observed during the whole electrochemical measurements and that the Pt real surface area of all the catalysts keeps an almost constant value even when cycling between 0.05 and 1.2 V/RHE, revealing thus that the catalysts are stable and that no change in the Pt/Cr ratio happens under these experimental conditions.

Figure 6 shows a comparison of the ORR on the Pt/C and Pt−Cr/C catalysts under similar experimental conditions. From the figure, the ORR on all the catalysts is diffusion controlled when the potential is less than 0.7 V and is under mixed diffusion kinetics control in the potential region between 0.7 and 0.85 V. In the Tafel region (potentials higher than 0.85 V) and the mixed potential region, it was found that the ORR activities of all the catalysts are roughly identical with respect to the MA of the total metal loading. On the basis of the MA of Pt, however, all the Pt−Cr alloy catalysts are slightly more active than the Pt/C catalyst for the ORR, which is qualitatively similar to the Pt−Ni and Pt−Co alloy catalysts (from E-Tek) recently reported by Paulus and co-workers.[38,39] Furthermore, the Koutecky−Levich plots (not shown in this paper) for the ORR on the different catalytic electrodes showed that all plots are straight lines with almost the same slope as that of the theoretically predicted line with four-electron reduction of oxygen, indicating that the oxygen reduction on all Pt-based

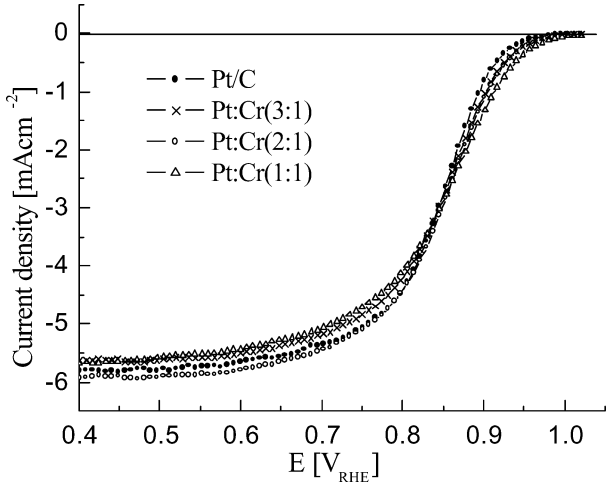


**Figure 6.** Linear scan voltammograms of the carbon-supported nanosized Pt and Pt−Cr alloy catalysts in 0.5 M $HClO_4$ saturated with pure oxygen at the scan rate of 5mV/s and the rotating speed of 2000 rpm. Current densities are normalized to the geometric surface area.

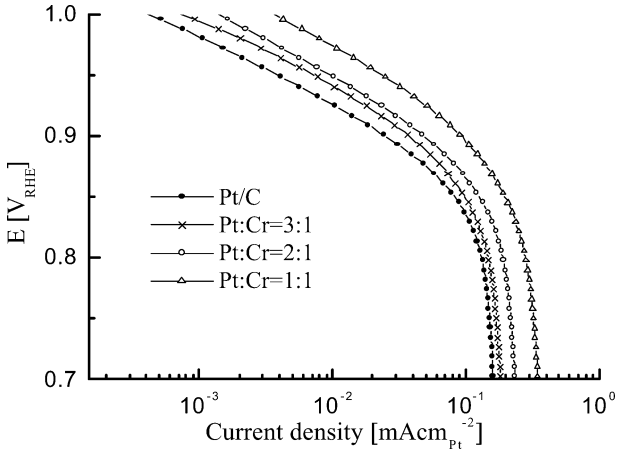


**Figure 7.** Tafel plots for the ORR on the different Pt-based catalysts in 0.5 M $HClO_4$ at the scan rate of 5 mV/s and the rotating speed of 2000 rpm. Current densities are normalized to the real surface area of platinum within the catalysts.

catalysts follows a four-electron process leading to water. It is worth mentioning that the open circuit potential of the Pt−Cr alloy catalysts in oxygen-saturated solution is slightly higher than that of the Pt/C catalyst, suggesting that the oxygen adsorption on the alloy surface is more favored than that on pure Pt surface.

To compare the specific activity (SA) of the different Pt-based catalysts for the ORR, Tafel plots of the kinetic current densities based on the real surface area of platinum within the catalysts are shown in Figure 7. From the figure, the Tafel slope can be obtained. The obtained Tafel slopes at high potentials (>0.85 V) for the Pt/C, Pt−Cr(3:1)/C, Pt−Cr(2:1)/C, and Pt−Cr(1:1)/C catalysts are 59, 58, 60, and 63 mV decade$^{-1}$, respectively. Within the fitting error, the Tafel slope did not show any dependence on the composition and structural parameters of the catalysts. Thus, it can be concluded that the reaction pathway and the rate-determining step are the same on all the catalysts investigated here. Furthermore, it is evident that the SA of the Pt−Cr alloy catalysts for the ORR is higher than that of the Pt/C catalyst and that the SA increases with increase of the Cr content. The kinetics enhancement for the ORR on the Pt−Cr alloy catalysts is a factor of 1.5−3, which depends on the catalyst composition. It should be mentioned that we did not find any kinetics enhancement of the ORR in

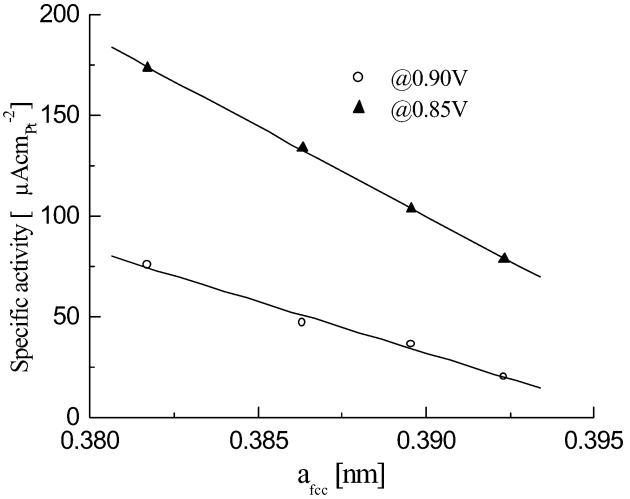


**Figure 8.** Relationships between the specific activities for the ORR on the Pt and Pt−Cr alloy catalysts and the lattice parameters. The fitted straight lines are also given in the figure.

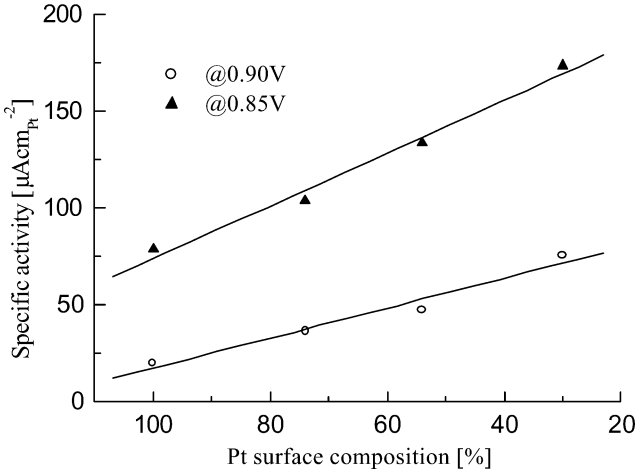


**Figure 9.** Relationships between the specific activities for the ORR on the Pt and homemade Pt−Cr alloy catalysts and the Pt surface composition. The fitted straight lines are also given in the figure.

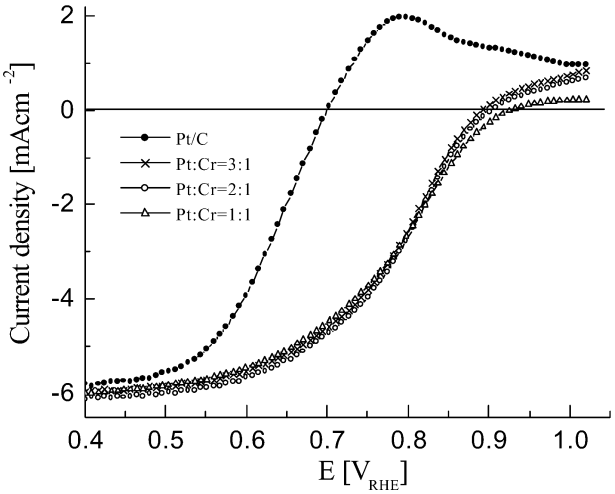


**Figure 10.** Linear scan voltammograms of the Pt/C catalyst and the carbon-supported nanosized Pt−Cr alloy catalysts in 0.5 M $HClO_4$ + 0.5 M $CH_3OH$ saturated with pure oxygen at the scan rate of 5 mV/s and the rotating speed of 2000 rpm.

pure sulfuric acid, probably due to the fact that the bisulfate adsorption ($HSO_4^-$) on the Pt−Cr alloy catalysts is stronger than that on pure Pt/C. As reported in the literature, a variety of Pt alloys (such as Pt−Cr, Pt−Co, Pt−Ni, and Pt−Fe) have been investigated for the ORR both in phosphoric acid fuel cells and PEMFCs. In general, most of the authors reported an activity enhancement of the ORR on the alloy catalysts with factors of 1.5−3 in comparison to pure Pt. However, it should be pointed out that these results on the Pt alloy catalysts for the ORR are by no means consistent. For example, Glass et al.[60] reported that the Pt−Cr alloy for the ORR is less active than pure Pt in phosphoric acid media. This may be due to the bulk nature of the electrodes used in their study. Beard and Ross[31] found that the SA of the Pt−Co alloy is lower than that of pure Pt and that the stability is not as good as pure Pt. This can be due to the particle size effect between Pt and Pt−Co alloy catalysts.

It is well known that, for the electrochemical reaction, the structure and surface composition of the catalysts are two key points in determining the adsorption/catalytic properties. Generally, the activity enhancement in the ORR on Pt-based alloy catalysts could be ascribed to the changes in structural parameters (such as lattice parameter and Pt−Pt interatomic distance). Thus, the increase in the SA with the homemade Pt−Cr alloy catalysts could be correlated to the change in the lattice parameters. Figure 8 shows the relationship between the specific activities at 0.90 and 0.85 V for the ORR on the Pt and Pt−Cr alloy catalysts and the lattice parameter. This plot shows a good linearity, that is, the specific activities at 0.90 and 0.85 V for the ORR linearly increase with the decrease of the lattice parameters, which is in good agreement with the previously published results,[40,61] indicating that the structural parameter of the Pt-based catalysts may play an important role in determining the oxygen adsorption and the kinetics of the ORR. Interestingly, the increase in the SA with the homemade Pt−Cr alloy catalysts is also linear with the change in Pt/Cr surface composition as shown in Figure 9, assessing that the surface composition is also an important factor in determining the ORR activity. Therefore, the SA enhancement of Pt for the ORR could be explained by a more favorable Pt−Pt interatomic distance for oxygen adsorption on the Pt−Cr alloys produced by the lattice contractions[30,40] and by the possible presence of oxygen species coordinated to the neighboring Cr atoms.

As mentioned above, the change in surface composition or of the Pt surface area may play an important role in the ORR electrocatalysis.[62] Thus, it is necessary to determine the possible changes in surface composition or if a surface segregation during the electrocatalytic process may take place. The real surface area of Pt within the Pt−Cr alloy catalyst before and after the electrochemical polarization at 0.80 V in oxygen-saturated perchloric acid solution for 1 h increased only ca. 2%, indicating that the stability of the alloy catalyst is good and that no Pt surface enrichment of the alloy catalysts does occur during the ORR. Thus, it is believed that the Pt/Cr surface composition almost keeps constant during the electrochemical measurements. However, spectroscopic investigations under in situ conditions are needed to assess this expectation.

**3.3. Electrochemical Behavior of the Catalysts for the ORR in Methanol-Containing Perchloric Acid Electrolyte.** It is known that the crossover of methanol from the anode to the Pt-based cathode can lead to a further reduction of the cell voltage by ca. 200−300 mV, particularly when air flows are used in DMFC. Thus, it is highly desirable to develop ORR electrocatalysts, which have a high methanol tolerance for DMFC applications. Figure 10 shows the ORR activity of the Pt/C catalyst and the homemade nanosized Pt−Cr alloy catalysts in the presence of 0.5 M $CH_3OH$. As compared to the ORR in pure $HClO_4$ solution (cf. Figure 6), all the catalysts for the ORR showed an increase in overpotential under the same current

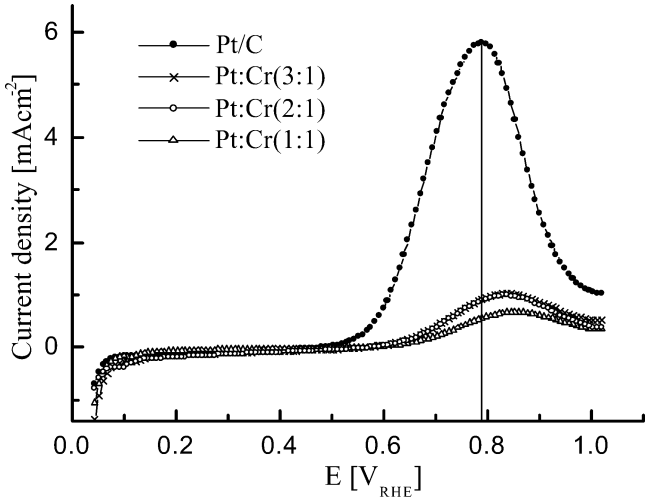


**Figure 11.** Linear scan voltammograms of the methanol oxidation on the Pt/C catalyst and the carbon nanosized Pt−Cr alloy catalysts in nitrogen saturated 0.5 M $HClO_4$ + 0.5 M $CH_3OH$ solution at the scan rate of 5 mV/s and the rotating speed of 2000 rpm.

density in the presence of methanol. For the ORR on pure Pt catalyst in methanol-containing solution, the overpotential increases by ca. 200 mV and the onset potential increases by ca. 300 mV. The significant increase in overpotential of the ORR on pure Pt catalyst is due to the competitive reaction between oxygen reduction and methanol oxidation (MOR). By use of the Pt−Cr alloy catalysts, there is also a decrease of the activity for the ORR in methanol-containing electrolyte. The apparent potential loss (around 70 mV) is due to mixed potential of ORR and MOR. From the figure, it is very clear that the ORR activity (both in MA and SA) on the Pt−Cr alloy catalysts in methanol-containing solution is much higher than that on pure Pt, indicating that the Pt−Cr alloys are methanol-tolerant catalysts during the ORR in contrast to pure Pt catalyst. Meanwhile, the current density of methanol oxidation in oxygen saturated solution on the alloy catalysts at high potentials (above 0.85 V) is lower than on pure Pt catalyst, and it decreases with the increase of the Cr content. Furthermore, all the Pt−Cr alloy catalysts showed nearly the similar MA for the ORR in the presence of methanol, which is consistent with that in pure acid solution. Considering the MA and SA of Pt, however, the Pt−Cr(1:1)/C catalyst appears to be the most active for the ORR in methanol-containing solution. Moreover, it can be compared with the previously published results that the ORR activity on the Pt−Cr alloy catalysts is higher than that on the ruthenium based transition metal chalcogenide catalysts[26] and the transition metal macrocycles,[20,22] which are inactive for the oxidation of methanol.

As recently reported in our laboratory,[28] it was found that the particle size of a pure Pt catalyst has a significant influence on the ORR activity both in the absence and presence of methanol. In methanol-containing solution, it was found that pure Pt catalyst with small particle size showed an increased methanol-tolerance for the ORR. In our study, it can be seen from Table 2 that the mean particle size of all the alloy catalysts is larger than that of pure Pt catalyst, clearly indicating that the high methanol-tolerance of the Pt−Cr catalysts for the ORR is mainly due to the alloying effect. To understand the origin of the high methanol tolerance of Pt−Cr alloy catalysts during the ORR, the methanol oxidation in $N_2$ saturated solution was studied under similar experimental conditions. Figure 11 shows the linear scan voltammograms of the methanol oxidation on

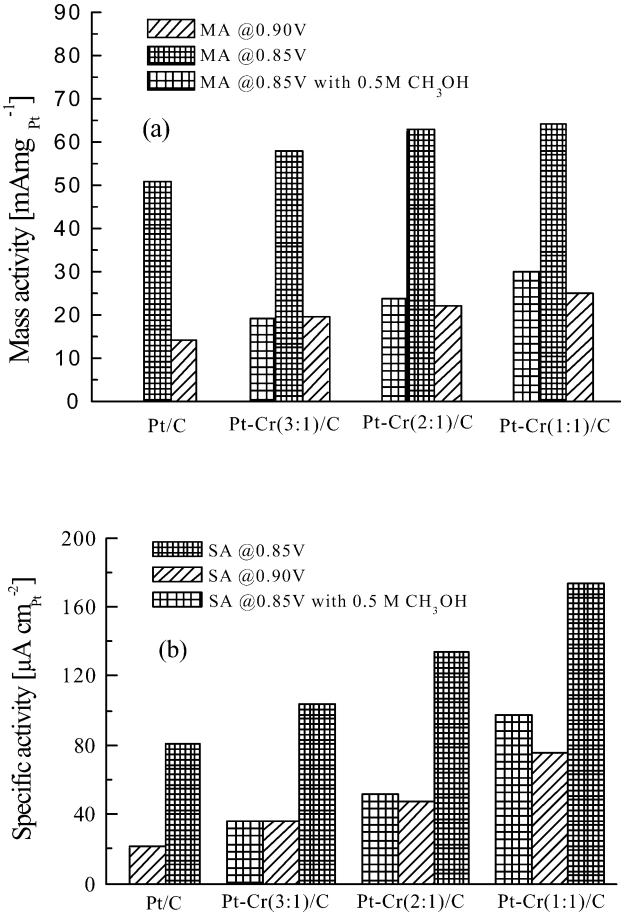


**Figure 12.** Histograms of the MA (a) and the SA (b) of the Pt-based catalysts for the ORR in 0.5 M $HClO_4$ solution.

the Pt/C catalyst and the carbon-supported nanosized Pt−Cr alloy catalysts in nitrogen saturated 0.5 M $HClO_4$ + 0.5 M $CH_3OH$ solution. It can be seen that the current densities of the methanol oxidation reaction on Pt−Cr alloy catalysts are much lower than that on Pt/C catalyst and that the methanol oxidation peaks on Pt−Cr alloy catalysts shift to more positive potentials as compared to the Pt/C catalyst, indicating that the alloy catalysts for methanol oxidation are less active than the Pt/C catalyst. This fact could explain the high methanol tolerance of the Pt−Cr alloy catalysts during the ORR. It is well established that for methanol oxidation at least three adjacent Pt sites in the proper crystallographic arrangement are necessary to activate the chemisorption of methanol.[5,63,64] For the Pt−Cr alloy catalysts with a disordered structure, the probability of finding three neighboring Pt atoms on the surface is lower if no Pt enrichment on the surface does take place. The Pt/Cr surface composition analysis of all Pt−Cr alloy catalysts in Table 2 reveals that the homemade alloy catalysts have Cr enrichment on the surface. Thus the surface composition is very probably different from the bulk. Unfortunately, this kind of information is difficult to obtain. This can explain the fact that all the Pt−Cr alloy catalysts have low activity for methanol oxidation and thus high methanol tolerance during the ORR. Therefore, the high activity of these methanol-tolerant catalysts for oxygen reduction could be ascribed to the composition effect (especially surface composition effect) and the disordered surface structure of the Pt−Cr alloy catalysts. Of course, a good dispersion of the Pt−Cr alloy catalysts in this work is also an important factor to determine their activity for oxygen reduction in the presence of methanol. Both effects can be separated by deconvoluted

method as performed on pure platinum supported electrodes.[65] The ORR and MOR processes show different electrochemical pathway as revealed by DEMS.[27]

Finally, the kinetics enhancement of the ORR in the absence and presence of methanol is summarized in Figure 12. Note that both the MA and SA of the Pt/C catalyst for the ORR are higher than the previously published results.[28,66] probably due to a better dispersion of our catalyst. It can be found that all Pt−Cr alloy catalysts showed slightly enhanced electrocatalytic activity for the ORR in the absence of methanol, and a significant enhancement in the electrocatalytic activity in the presence of methanol in comparison to pure Pt catalyst. Thus, the carbon-supported Pt−Cr alloy catalysts with the disordered structure and well-dispersed nanoparticles on Vulcan XC-72 carbon could be used in practical PEMFCs. The effects of temperature and metal loading of the as-prepared alloy catalysts on the electrocatalytic performances of the ORR in the absence and presence of methanol and its application in practical DMFC will be reported in another paper.

## 4. Conclusions

The ORR in the absence and presence of methanol on Vulcan XC-72 carbon-supported nanosized Pt−Cr alloy catalysts has been studied. The catalyst preparation procedure via the carbonyl route seems to be an efficient one to obtain Pt−Cr nanoparticles with a narrow particle size distribution and disordered surface structure. The carbon-supported Pt−Cr alloy catalysts with different Pt/Cr atomic ratios showed a slightly enhanced MA and a greater SA enhancement by a factor of 1.5−3 for the ORR in the absence of methanol, and a significant enhancement of the SA and MA in the presence of methanol as compared to the Pt/C catalyst. The high methanol tolerance of Pt−Cr alloy catalysts during the ORR can be explained well by the low activity of such catalysts for methanol oxidation, which could originate from the composition effect and the disordered surface structure of the as-prepared alloy catalysts.

**Acknowledgment.** The authors greatly acknowledge the French Fuel Cell Network and the Ministry of Research for their support in the framework of OPTIMET program (Research Grant No. 00S0060).

## References and Notes

(1) Arico, A.; Srinivasan, S.; Antonucci, V. *Fuel Cells* **2001**, *2*, 133.
(2) Wasmus, S.; Kuver, A. *J. Electroanal. Chem.* **1999**, *461*, 14.
(3) McNicol, B. D.; Rand, D. A. J.; Williams, K. R. *J. Power Sources* **1999**, *83*, 15.
(4) Kelley, K. C.; Deluga, G. A.; Smyrl, W. H. *Electrochem. Solid State Lett.* **1999**, *3*, 407.
(5) Lamy, C.; Lima, A.; Le Rhun, V.; Coutanceau, C.; Léger, J. M. *J. Power Sources* **2002**, *105*, 283.
(6) Hogarth, M. P.; Ralph, T. R. *Platinum Met. Rev.* **2002**, *46*, 146.
(7) Iwasita, T.; Nart, F. C. *J. Electroanal. Chem.* **1991**, *317*, 291.
(8) Jarvi, T. D.; Sriramulu, S.; Stuve, E. M. *J. Phys. Chem. B* **1997**, *101*, 3646.
(9) Reddington, E.; Sapienza, A.; Smotkin, E. S. et al. *Science* **1998**, *280*, 1735.
(10) Ralph, T. R.; Hogarth, M. P. *Platinum Met. Rev.* **2002**, *46*, 3.
(11) Paffet, M. T.; Beery, G. J.; Gottesfeld, S. *J. Electrochem. Soc.* **1998,** *135*, 1431.
(12) Freund, F.; Lang, J.; Lehman, T.; Starz, K. A. *Catal. Today* **1996**, *27*, 279.
(13) Ren, X.; Zelenay, S.; Thomas, S.; Davey, J.; Gottesfeld, S. *J. Power Sources* **2000**, *86*, 111.
(14) Kauranen, P. S.; Skou, E. *J. Electroanal. Chem.*, **1996**, *408*, 189.
(15) Gurau, B.; Smotkin, E. S. *J. Power Sources* **2002**, *112*, 339.
(16) Arico, A.; Creti, P.; Antonucci, P. L.; Antonucci, V. *Electrochem. Solid-State Lett.* **1998**, *1*, 66.
(17) Bittins-Cattaneo, B.; Wasmus, S.; Vielstich, W. *J. Appl. Electrochem.* **1993,** *23*, 625.
(18) Ravikumar, M. K.; Shukla, A. *J. Electrochem. Soc.* **1996,** *173*, 2601.
(19) Chu, D.; Gilman, S. *J. Electrochem. Soc.* **1994**, *147*, 4605.
(20) Jiang, R. Z.; Chu, D. Y. *J. Electrochem. Soc.* **2000**, *147*, 4605.
(21) El Hourch, A.; Coutanceau, C.; Léger, J. M.; Lamy, C. *J. Electroanal. Chem.* **1997,** *426*, 117.
(22) Convert, P.; Coutanceau, C.; Gloaguen, F.; Lamy, C. *J. Appl. Electrohem.* **2001,** *31*, 945.
(23) Alonso-Vante, N.; Tributsch, H. *Nature* **1986,** *323*, 431.
(24) Alonso-Vante, N. *J. Chim. Phys.* **1996,** *93*, 702.
(25) Schmidt, T. J.; Paulus, U. A.; Gasteiger, H. A.; Alonso-Vante, N.; Behm, R. J. *J. Electrochem. Soc.* **2000**, *147*, 2620.
(26) Bron, M.; Bogdanoff, P.; Fiechter, S.; Hilgendorff, M. *J. Electroanal. Chem.* **2001,** *517*, 85.
(27) Alonso-Vante, N.; Bogdanoff, P.; Tributsch, H. *J. Catal.* **2000,** *190*, 240.
(28) Maillard, F.; Martin, M.; Gloaguen, F.; Léger, J. M. *Electrochim. Acta* **2002**, *47*, 3431.
(29) Drillet, J. F.; Ee, A.; Friedemnan, J.; Kotz, R.; Schmidt, V. M. *Electrochim. Acta* **2002**, *47*, 1983.
(30) Stamenkovic, V.; Schmidt, T. J.; Ross, Ph.; Markovic, N. M. *J. Phys. Chem. B* **2002**, *106*, 11970.
(31) Beard, B. C.; Ross, P. N. *J. Electrochem. Soc.* **1990,** *137*, 3368.
(32) Mukerjee, S.; Srinivasan, S. *J. Electroanal. Chem.* **1993,** *357*, 201.
(33) Min, M. K.; Cho, J.; Cho, K.; Kim, H. *Electrochim. Acta* **2000,** *45*, 4211.
(34) Mukerjee, S.; Srinivasan, S.; M. P. Soriaga, M. P. *J. Phys. Chem. B* **1995,** *99*, 4577.
(35) Mukerjee, S.; Srinivasan, S.; M. P. Soriaga, M. P.; McBreen, J. *J. Electrochem. Soc.* **1995,** *142*, 1409.
(36) Toda, T.; Igarashi, H.; Uchida, H.; Watanabe, M. *J. Electrochem. Soc.* **1999,** *146*, 3750.
(37) Tamizhmari, G.; Capuano, G. A. *J. Electrochem. Soc.* **1994,** *141*, 968.
(38) Paulus, U. A.; Wokaun, A.; Scherer, G. G.; Schmidt, T. J.; Stamenkovic, V.; Markovic, N. M.; Ross, P. N. *J. Phys. Chem. B* **2002**, *106*, 4181.
(39) Paulus, U. A.; Wokaun, A.; Scherer, G. G.; Schmidt, T. J.; Stamenkovic, V.; Markovic, N. M.; Ross, P. N. *Electrochim. Acta* **2002**, *47*, 3787.
(40) Antolini, E.; Passos, R. R.; Ticianelli, E. A. *Electrochim. Acta* **2002**, *48*, 263.
(41) Park, K. W.; Choi, J. H.; Kwon, B. K.; Lee, S. A.; Sung, Y. E.; Ha, H. Y.; Hong, S. A.; Kim, H. S.; Wieckowski, A. *J. Phys. Chem. B* **2002**, *106*, 1869.
(42) Xiong, L.; Kannan, A. M.; Manthiram, A. *Electrochem. Comm.* **2002,** *4*, 898.
(43) Sun, S.; Murray, C. B.; Weller, D.; Folks, L.; Moser, A. *Science* **2000**, *287*, 1989.
(44) Ould Ely, T.; Pan, C.; Amiens, C.; Chaudret, B.; Dassenoy, F.; Lecante, P.; Casanove, M. J.; Mosset, A.; Respaund, M.; Broto, J. M. *J. Phys. Chem. B* **2000**, *104*, 695.
(45) Park, J. I.; Cheon, J. *J. Am. Chem. Soc.* **2001**, *123*, 5743.
(46) Ono, K.; Okuda, R.; Ishii, Y.; Kamimura, S.; Oshima, M. *J. Phys. Chem. B* **2003**, *107*, 1941.
(47) Dassenoy, F.; Vogel, W.; Alonso-Vante, N. *J. Phys. Chem. B* **2002**, *106*, 12152.
(48) Nasher, M. S.; Frenkel, A. I.; Somerville, D.; Hills, C. W.; Shapley, J. R.; Nuzzo, R. G. *J. Am. Chem. Soc.* **1998**, *120*, 8093.
(49) Hills, C. W.; Nasher, M. S.; Frenkel, A. I.; Shapley, J. R.; Nuzzo, R. G. *Langmuir* **1999**, *15*, 690.
(50) Dickinson, A. J.; Carrette, L. P. L.; Collins, J. A.; Friedrich, K. A.; Stimming, U. *Electrochim. Acta* **2002**, *47*, 3733.
(51) Manzo-Robledo, A.; Boucher, A. C.; Pastor, E.; Alonso-Vante, N. *Fuel cells*, **2002,** *2*, 109. (b) Boucher, A. C.; Alonso-Vante, N.; Dassenoy, F.; Vogel, W. *Langmuir* **2003**, *19*, 10885.
(52) Stonehart, P. *Ber. Bunsen-Ges. Phys. Chem.* **1990**, *94*, 913.
(53) Longoni, G.; Chini, P. *J. Am. Chem. Soc.* **1976**, *98*, 7225.
(54) Pozio, A.; Francesco, M. D.; Cemmi, A.; Giorgi, L. *J. Power Sources* **2002**, *105*, 13.
(55) Shim, J.; Yoo, D. Y.; Lee, J. S. *Electrochim. Acta* **2000**, *45*, 1943 and references therein.
(56) Antolini, E. *Mater. Chem. Phys.* **2003,** *78*, 563.
(57) Matyi, R. J.; Schwartz, L. H.; Butt, J. B. *Catal. Rev.−Sci. Eng.* **1987,** *29*, 41.
(58) Borodzinski, A.; Bonarowska, M. *Langmuir* **1997,** *13*, 5613.
(59) Anderson, A. *Electrochim. Acta* **2002**, *47*, 3759.

(60) Glass, J. T.; Cahen, G. L.; Stoner, G. E.; Taylor, E. J. *J. Electrochem. Soc.* **1987,** *134*, 58.
(61) Kim, K. T.; Kim, Y. G.; Chung, J. S. *J. Electrochem. Soc.* **1995,** *142*, 1531
(62) Markovic, N. M.; Ross, P. N. *Surf. Sci. Rep.* **2002,** *45*, 117.
(63) Gasteiger, H. A.; Markovic, N.; Ross, P. N., Jr.; Cairns, E. J. *J. Electrochem. Soc.* **1994,** *141*, 1795.
(64) Gasteiger, H. A.; Markovic, N.; Ross, P. N., Jr.; Cairns, E. J. *Electrochim. Acta* **1994,** *39*, 1825.
(65) Paulus U. A.; Schmidt, T. J.; Gasteigert, H. In *Handbook of Fuel Cells: Fundamentals, Technology, and Applications*; Vielstich, W., Lamm, A., Gasteiger, H. A., Eds.; Wiley: New York, 2003; Vol. 2, Chapter 38, p 555.
(66) Antoine, O.; Bultel, Y.; Durand, R. *J. Electroanal. Chem.* **2001,** *499*, 85.